Chapter 2 Magnetic transitions in $BiFeO_3$

2.1. Introduction

Bismuth ferrite ($BiFeO_3$) is one of the most investigated magneto-electric multiferroics because of its room temperature multiferroicity with potential for applications in multifunctional devices of technological importance [29,32,34,68,95]. The room temperature ferroelectric phase of bulk $BiFeO_3$ corresponds to a rhombohedrally distorted perovskite structure in the *R*3c space group [74] in which the cations are displaced with respect to the anions along the [111] direction while the neighbouring oxygen octahedra are rotated in opposite directions (antiphase tilted structure in the $a^-a^-a^-$ tilt system [204]) about the same direction. The ferroelectric phase transition temperature is reported to be T_C ~ 1103 K [65]. The magnetic structure of $BiFeO_3$ corresponds to a non-collinear *G*-type antiferromagnetic (AFM) ordering with a superimposed incommensurate magnetic modulation below the Neel temperature T_N ~ 643 K [66]. While the nuclear and magnetic structures as well as the multiferroic properties of $BiFeO_3$ at and above the room temperature are well settled, [68,95] there exists considerable controversy about the low temperature phase transitions in this compound [87,102–104,108,109,111,112,114–117]**.**

Historically, the first low temperature magnetic transition in $BiFeO_3$ was reported by Nakamura et al. [108] using splat quenched samples. Their results showed a frequency dependent cusp in ac susceptibility ($\chi'(\omega, T)$) around T_f ~21 K with a spin-glass (SG) transition temperature T_{SG} ~ 14 K. Recent $\chi(\omega, T)$ measurements on single crystals of $BiFeO_3$ by Singh et al. [102] have also revealed frequency dependent cusp similar to that reported by Nakamura et al. [108], though with a slightly higher cusp temperature (T_f ~25 K), but with the T_{SG} ~ 29.4 K greater than T_f ~ 25 K, which is physically unrealistic as T_{SG} is the cusp temperature corresponding to the limit of $\omega (=2\pi f) \rightarrow 0$. In fact, T_{SG} in the

canonical and cluster spin glasses is invariably lower than the cusp temperature (T_f) measured at various frequencies [24,41,42]. Further, the χ (ω, T) data presented by Singh et al. [102] is also intriguing on two counts. Firstly, the peak height of χ' (ω, T) increases with increasing frequencies (see Fig. 4(a) of Ref. [102]) which is unusual as the susceptibility always decreases with increasing frequency. This anomalous frequency dependence has been attributed by Singh et al. [102] to the measuring frequency being close to the inverse of the time constant of the lumped equivalent RC circuit of the sample. The measured imaginary part of ac susceptibility, i.e. $\chi''(\omega, T)$, is also physically unrealistic as it is shown to be negative near the cusp temperature range. According to Singh et al. [102], the negative cusps at T_f in the χ'' (ω, T) may be linked with the modulated magnetic structure of $BiFeO_3$. Surprisingly, the low temperature zero field cooled (ZFC) and field cooled (FC) dc magnetization (M (T)) measurements by various workers have not revealed any signature of a spin-glass transition around 25 K and its existence has been identified by $\chi(\omega, T)$ measurements, [102] dielectric ($\varepsilon(\omega, T)$) measurements [110] and Raman studies [110] only.

In addition to the SG transition, several other transitions have been reported in $BiFeO_3$ using different measurement probes. ZFC M(T) measurements on polycrystalline powders of $BiFeO_3$ have revealed anomalies around 50 K [87], 150 K [103] and 250 K [103]. Further, the ZFC and FC M (T) curves have been reported to bifurcate below 300 K and the anomaly around 50 K does not appear under the FC condition. This has been taken as evidence for SG freezing or superparamagnetic (SPM) blocking [87,102]. The anomaly around 50 K has also been reported in the ZFC M(T) measurements on single crystals [102] as well as nanocrystalline powders [87,104].

Differential scanning calorimetry (DSC) measurements on polycrystalline $BiFeO_3$ have revealed a strong specific heat anomaly at ~250K around which an anomaly in ZFC

M (T) has also been reported [103]. The differential thermal analysis (DTA) measurements on $BiFeO_3$ single crystals, on the other hand, do not reveal any anomaly around 250 K but reveals the possibility of another phase transition in the 140 to 150 K range with a latent heat [109]. Temperature dependence of the magnetic entropy, as obtained by DSC measurements, indicates as many as five phase transitions occurring at ~38 K, ~150 K, ~178 K, ~223 K and ~250 K [103]. The ε (ω, T) measurements reveal weak anomalies around 55 K, 140 K and 215 K for single crystals [109] and around 25 K [110], 50 K [109], 200 K [109] and 220-260 K [109,117] in ceramics. Elastic modulus measurements have revealed anomalies around 140 K [109,115] and 200 K [109], respectively. Further, Raman spectroscopic studies on polycrystalline and single crystals of $BiFeO_3$ have revealed transitions at 25 K [110], 90 K [112], 140 K [111–116], 200 K [111–113] and 250 K [112]. Redfern et al. [109] have attributed the transitions occurring around 38-50 K, 140–150 K and 220–250 K to be magnetic but glassy with magnetoelectric coupling, predominantly magnetic involving spin reorientation and AFM to SG transition with weak coupling with polarization, respectively [109]. Further, the transition around 178–200 K has been proposed to be magnetoelastic in nature with a small coupling to polarization [109].

It is evident from the foregoing that no single research group has reported all the low temperature transitions in the same sample. Further, no single technique has revealed so far all the transitions. The fact that Nakamura et al. [108] did not find any cusp in χ (ω, T) around T_f ~ 50 K or signatures of other transitions above 50 K in splat quenched $BiFeO_3$ samples, supposed to be free from oxygen ion vacancies, also raises doubts about the intrinsic nature of various low temperature transitions other than the transition occurring around 25 K. In this chapter, the results of a comparative study of undoped and Mn-doped $BiFeO_3$ are presented to understand the effect of Mn-doping in small

concentration (1.5 at%) on the (1) oxygen ion vacancy concentration and the associated redox reactions, on one hand, and (2) low temperature magnetic phase transitions of $BiFeO_3$, on the other.

2.2. Sample preparation:

Both undoped and Mn-doped $BiFeO_3$ powders were prepared by the conventional solid-state route using high purity oxides as starting materials: Bi_2O_3 (Aldrich, 99.9 %), Fe_2O_3 (Aldrich, 99 %) and MnO_2 (Alfa Aesar, 99.9%). We have added 0.3 wt% MnO_2 during calcination for the preparation of doped samples. The ingredient powders were taken in stoichiometric proportions and mixed in an agate mortar pestle for 3 hours and subsequently in a planetary ball mill using a zirconia zar and zirconia balls for 6 hours with acetone as the mixing media. After drying, the mixed powders were calcined at an optimized temperature of 1063 K for 8 hours in an open alumina crucible. The calcined powder was crushed and again ball milled for 4 hours. The powder so obtained was pressed at a load of 70 KN into disks of 13mm diameter and about 1mm thickness in a hydraulic press using steel die. 2% aqueous solution of polyvinyl alcohol (PVA) was used as a binder before pressing. After binder burn-off at 773 K for 10 hours, sintering was carried out at 1093 K for 1 hour in closed alumina crucibles with calcined powder of the same composition as spacer powder for preventing the loss of Bi_2O_3 during sintering.

2.3. Characterizations tools:

The microstructure and chemical composition of the sample was obtained using Scanning Electron Microscope (SEM) (Zeiss, model no. EVO 18) and Energy Dispersive X-ray spectroscopy (EDX) attachment (Oxford, model no. 51-ADD0048). The sintered pellet was coated with conducting gold using sputter coater (Royal life Sciences, model

no. DSR1) under vacuum before taking the SEM images. The oxygen stoichiometry was determined by iodometric titration method.

The room temperature high-resolution synchrotron x-ray powder diffraction (SXRD) data were collected at P02.1 beamline of PETRA III, Hamburg, Germany, at a wavelength of 0.2079Å (~60keV). The powder sample was filled in a Kapton capillary of 0.8mm diameter and exposed for 10 s by the incident beam of cross section 0.5 mm × 0.5 mm. Two-dimensional (2D) x-ray powder diffraction (XRD) pattern was recorded using a Perkin Elmer 1621 Detector (2048 pixels × 2048 pixels, 200μm × 200μm pixel size). The sample to detector distance was set to 1310 mm. The standard LaB_6 was used to calibrate the sample to detector distance. The 2D XRD pattern was integrated using the FIT2D software. The XRD measurements were carried out using an 18-kW Cu-rotating anode based powder diffractometer (Rigaku, model no. RINT 2500/PC series) operating in the Bragg-Brentano geometry fitted with a curved crystal monochromator in the diffraction beam and a close cycle helium refrigerator based low temperature attachment. The data were collected in the 2θ range of 20 to 120 degrees at a step of 0.02 degrees. All the XRD patterns were recorded using powders obtained after crushing the ceramic pellets and annealing the crushed powder at 773 K for 10 hours for removal of stresses introduced during crushing.

X-ray photoelectron spectroscopy (XPS) measurements were performed using an Omicron energy analyzer (model no. EA-125) with Mg-K_α (1253.6 eV) lab source. The XPS data was analyzed by XPSPEAK 4.1 software.

The dc magnetization measurements were carried out using superconducting quantum interference device (SQUID) based magnetometer (Quantum Design, model no. MPMS-3) under zero filed cooled (ZFC) and field cooled (FC) conditions from 2K to 300K with low temperature attachment and ZFC M(T) from 300K to 750K using high temperature

attachment. For the ZFC measurements, the sample was first cooled from room temperature down to 2K in the absence of a magnetic field and the magnetization was measured in warming cycle after applying the magnetic field. For the FC measurements, the sample was cooled from room temperature down to 2K in the presence of magnetic field and magnetization was measured in the warming cycle under the same field.

For the resistivity and dielectric measurements, the pellets were gently polished with 0.25μm size diamond paste. After then acetone was used to clean the surfaces and then isopropyl alcohol was put on to remove the moisture on the surfaces. The electroding of the pellets on both sides was done using fired-on silver paste which is cured at 773K for 5 minutes. The DC resistivity of samples was measured using an electrometer (Keithley, model no. 6517A). The low temperature dielectric ($\varepsilon(\omega, T)$) measurements were carried out using the sample holder mounted on a variable temperature insert of a cryogen free measurement system (CFMS) (Cryogenic, model no. 7 Tesla mini CFM). Novocontrol (Alpha-A) high performance frequency analyzer was used for measuring the capacitance and loss tangent ($\tan\delta$).

2.4. Results and discussion:

2.4.1 Compositional analysis:

The composition was checked over individual grains and around grain boundaries separately. Fig. 2.1 (a-d) show the microstructure and the EDX spectra for the undoped and Mn-doped $BiFeO_3$ samples. The representative regions in the grain and at the grain boundaries are marked in the microstructures. The results of EDX analysis for the two types of samples are given in Table 2.1. Similar analyses were carried out at five randomly selected regions and the average composition is given in Table 2.2 for the undoped and Mn-doped samples. It is evident from these tables that the average composition obtained by EDX analysis is close to the nominal (expected) composition

within the limit of standard deviation for Bi, Fe and Mn. The oxygen content for the undoped sample is found to be a little less than that for the Mn-doped sample.

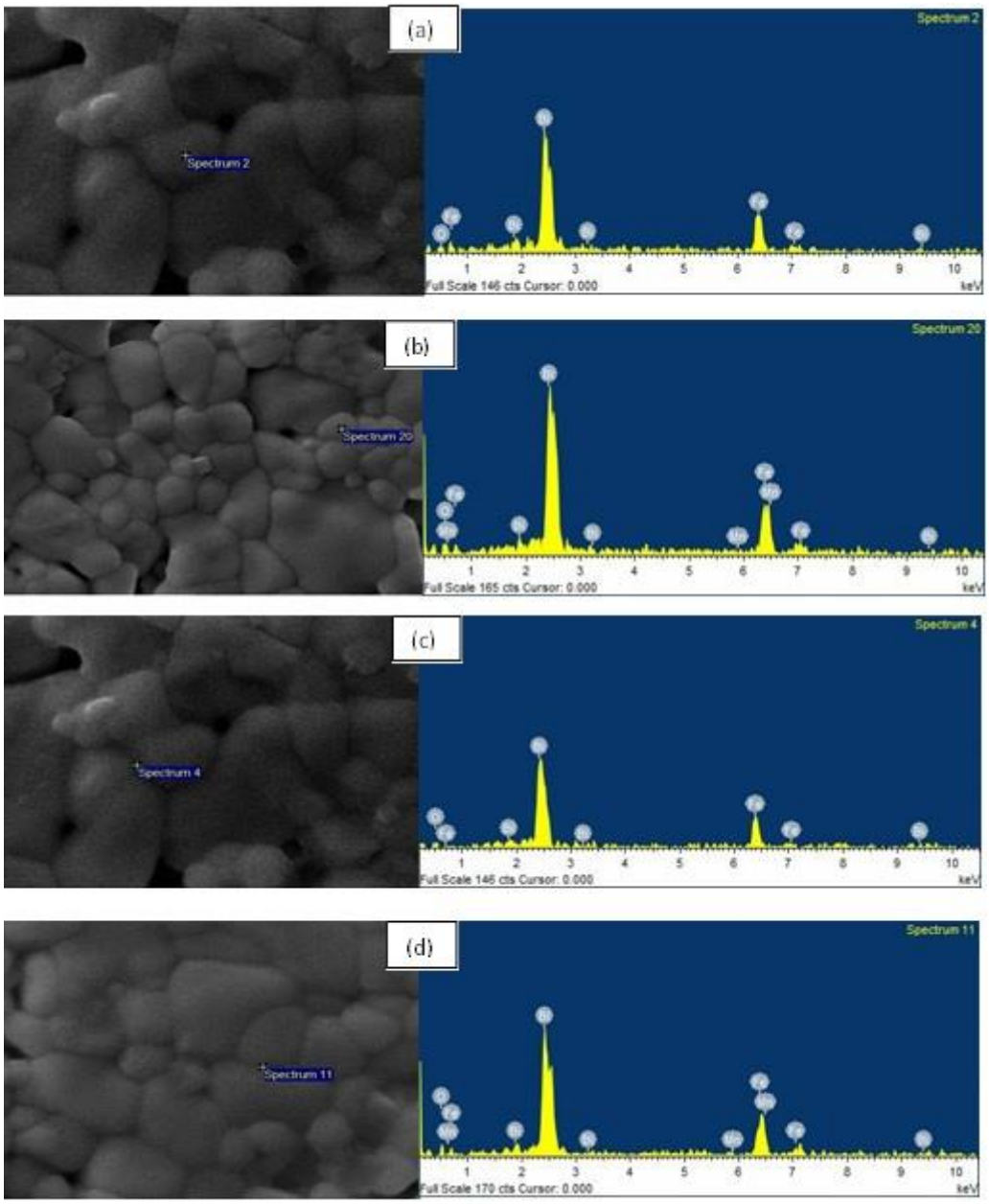

Figure 2.1: Microstructure and EDX spectra for undoped and Mn-doped $BiFeO_3$ **(a, b)** in the grain and **(c, d)** around the grain boundary.

However, it is worth mentioning that EDX is not the ideal tool for the determination of oxygen content. The oxygen content can be determined from the iodometric titration method and is found to be 2.94 ± 0.02 and 2.98 ± 0.02 for undoped and Mn-doped

$BiFeO_3$, respectively. The chemical composition formula for undoped and Mn-doped sample using EDX and iodometric titration analysis is found to be $BiFeO_{2.94\pm0.02}$ and $BiFe_{0.985}Mn_{0.015}O_{2.98\pm0.02}$, respectively.

Table 2.1: Results of EDX analysis of undoped and Mn-doped $BiFeO_3$ in weight percent and atomic percent for the microstructure and spectra shown in Fig. 2.1.

Undoped $BiFeO_3$					Mn-doped $BiFeO_3$				
	Chemical compositions					Chemical compositions			
	Grain		Grain Boundary			Grain		Grain Boundary	
Element	Weight %	Atomic %	Weight %	Atomic %	Element	Weight %	Atomic %	Weight %	Atomic %
O	11.9	52.7	11.3	51.3	O	12.6	54.5	14.6	58.0
Fe	18.7	23.8	18.8	24.4	Mn	0.3	0.4	0.3	0.4
Bi	69.4	23.5	69.9	24.3	Fe	17.6	21.9	18.5	21.2
					Bi	69.5	23.2	66.6	20.4

Table 2.2: Average composition of the undoped and Mn-doped $BiFeO_3$ samples in weight percent and atomic percent.

Undoped $BiFeO_3$			Mn-doped $BiFeO_3$		
	Average chemical compositions			Average chemical compositions	
Element	Weight %	Atomic %	Element	Weight %	Atomic %
O	13.0 ± 1.7	55.0 ± 3.5	O	13.6 ± 1.4	56.5 ± 3.1
Fe	18.6 ± 0.3	22.7 ± 1.7	Mn	0.3 ± 0.1	0.4 ± 0.2
Bi	68.4 ± 1.5	22.3 ± 1.9	Fe	17.8 ± 0.7	21.3 ± 1.6
			Bi	68.3 ± 1.3	21.8 ± 1.5

2.4.2 Room temperature synchrotron x-ray diffraction studies:

Single-phase powder and sintered ceramic samples of $BiFeO_3$ are rather difficult to prepare because of the narrow temperature range of the stability of the perovskite phase

and the volatile nature of Bi^{3+} that promotes the formation of impurity phases like $Bi_2Fe_4O_9$ [70] and $Bi_{25}FeO_{39}$ [71]. Figs. 2.2(a) and (b) compare the room-temperature SXRD patterns of undoped and Mn-doped $BiFeO_3$ powders. It is evident from the figures that both the samples are almost single phase as all the peaks correspond to the main perovskite phase of $BiFeO_3$ with only a trace amount of an impurity phase $Bi_2Fe_4O_9$ is present with a peak intensity that is 2.4 % of the strongest 220_{pc} peak of $BiFeO_3$ with respect to the doubled pseudocubic (pc) unit cell.

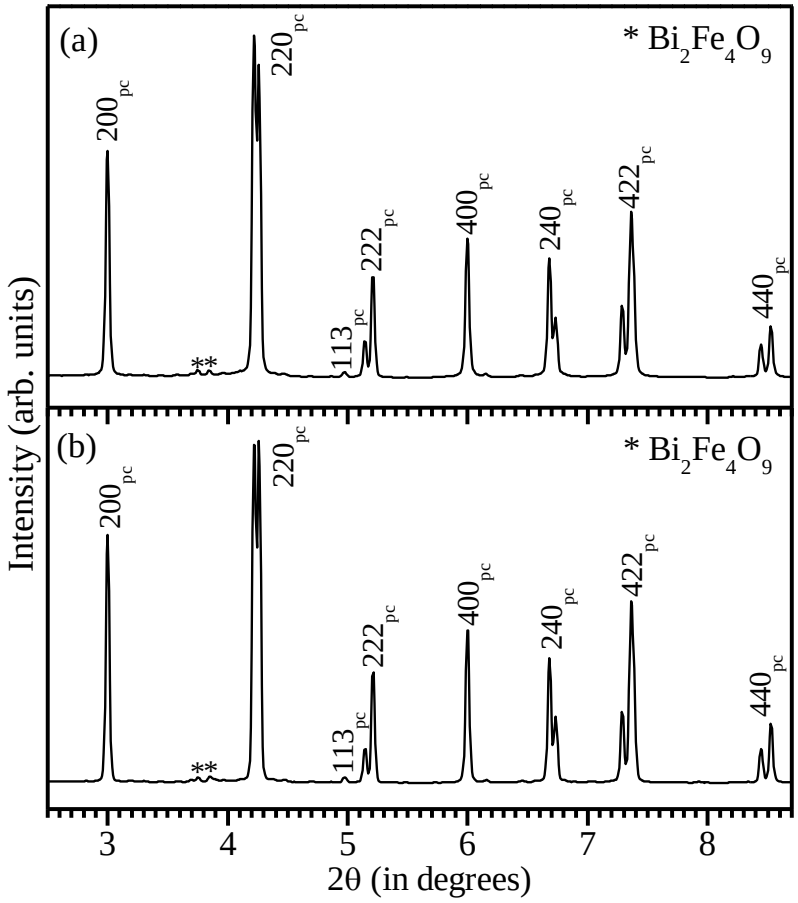

Figure 2.2: High resolution synchrotron x-ray powder diffraction patterns collected at room temperature for (a) Undoped $BiFeO_3$ and (b) Mn-doped $BiFeO_3$. All indices are with respect to a doubled pseudocubic cell.

It is also evident from Fig. 2.2(a) and (b) that the 400_{pc} is a singlet while 222_{pc} and 440_{pc} are doublets, as expected for the stable rhombohedral phase of $BiFeO_3$ in the R3c space group. The above qualitative observations for both the samples were further

confirmed by using the Rietveld refinement technique. For the Rietveld refinement of the rhombohedral phase of $BiFeO_3$ with R3c space group, we have used the hexagonal unit cell. In the asymmetric unit of $BiFeO_3$, the Bi^{3+} ions occupy the 6(a) Wyckoff site with (0, 0, 0) position and Fe^{3+} ions occupy the same 6(a) Wyckoff site with position (0, 0, z) while O^{2-} ions at the 18(b) Wyckoff site with position (x, y, z).

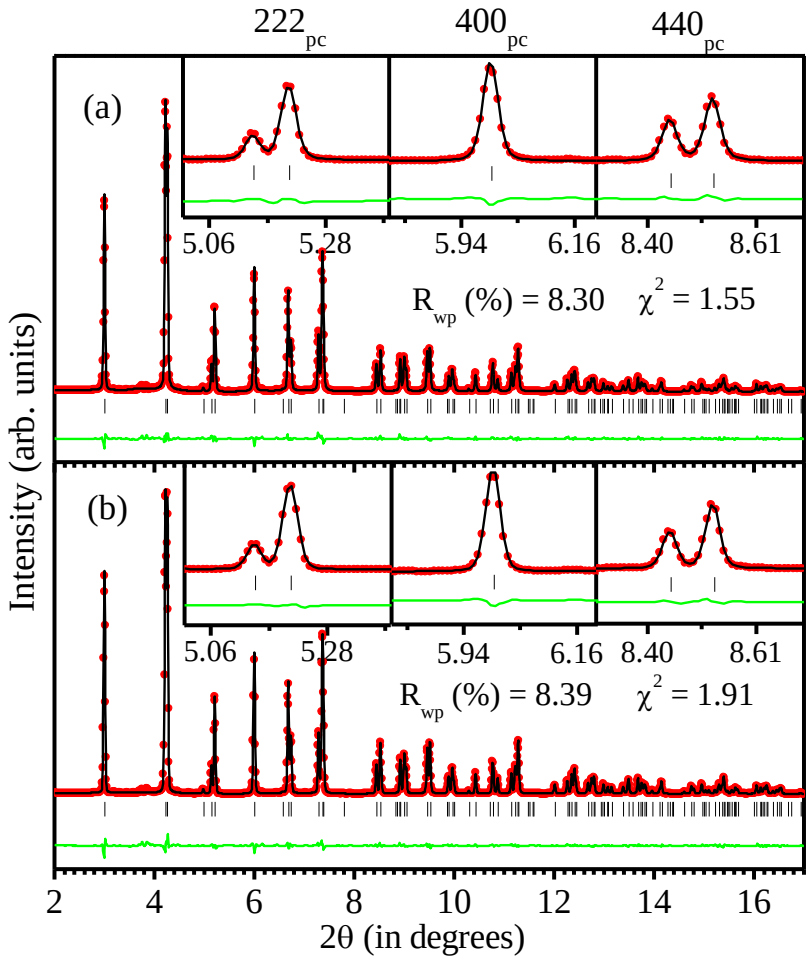

Figure 2.3: Observed (filled circles), calculated (continuous line), and difference (bottom line) profiles obtained from the Rietveld analysis of the room temperature synchrotron x-ray powder diffraction data for (a) Undoped $BiFeO_3$ and (b) Mn-doped $BiFeO_3$ sample using R3c space group. The vertical tick marks above the difference profile represent the Bragg peak positions. Insets depicts the profile fits for 222_{pc}, 400_{pc}, and 440_{pc} pseudocubic peaks.

In the refinement process the background was modelled with linear interpolation and the peak shape was modelled using pseudo-Voigt function. Occupancy of all the ions

were fixed at the nominal composition in the refinements. Zero correction, scale factor, background, lattice parameters, half width parameters (u, v and w), positional coordinates and thermal parameters were varied during the refinement. Fig. 2.3(a) and (b) depicts the Rietveld refinement of the SXRD patterns of undoped and Mn-doped $BiFeO_3$ samples at room temperature using R3c space group. It is evident from the figure that the observed (filled-circles) and calculated (continuous line) profiles show excellent fit, as can be seen from the difference (bottom line) profile given in this figure. This confirms that all the peaks in the SXRD patterns of both the samples are indexed with single phase of rhombohedral structure with R3c space group.

The refined structural parameters given in Table 2.3 are in good agreement with those reported in literature [205]. The important inference is that the unit cell parameters are not affected by Mn-doping.

Table 2.3: Structural parameters and agreement factors obtained from Rietveld refinement of SXRD data for undoped and Mn-doped $BiFeO_3$ sample using R3c space group.

Parameters	**Undoped $BiFeO_3$**	**Mn-doped $BiFeO_3$**	**Literature** [205]
a_{hex} (Å)	5.5782 (6)	5.5779 (8)	5.57874 (16)
c_{hex} (Å)	13.8665 (2)	13.8662 (3)	13.8688 (3)
v_{hex} (Å)	373.67 (8)	373.63 (1)	373.802 (17)
α, β, γ	$\alpha=\beta=90^0$, $\gamma=120^0$	$\alpha=\beta=90^0$, $\gamma=120^0$	$\alpha=\beta=90^0$, $\gamma=120^0$
Bi (x, y, z)	0	0	0
Fe (0, 0, z)	0.2208 (1)	0.2209 (2)	0.22077 (8)
O (x)	0.4481 (2)	0.4525 (1)	0.4428 (11)
O (y)	0.0179 (2)	0.0226 (2)	0.0187 (10)
O (z)	0.9536 (5)	0.9523 (6)	0.9520 (4)
β_{Bi}(Å^2)	0.64 (1)	0.64 (2)	$\beta_{11} = \beta_{22} = 0.00996$ (15) β_{33}=0.00641 (14)
β_{Fe} (Å^2)	0.43 (5)	0.44 (5)	$\beta_{11} = \beta_{22} = 0.00659$ (23), β_{33}=0.0054 (3)
β_O(Å^2)	0.63 (2)	0.67 (2)	$\beta_{11} = 0.0112$ (14), $\beta_{22} = \beta_{33}$=0.0078 (14) $\beta_{12} = 0.0052$ (12), β_{13} =-0.002(11), β_{23}= -0.0017 (11)
R_{wp} (%)	8.30	8.39	
χ^2	1.55	1.91	

2.4.3 Role of Mn-doping on oxygen ion vacancies:

It is well known that the electrical and magnetic properties of undoped $BiFeO_3$ are strongly influenced by oxygen ion vacancies created during sintering of $BiFeO_3$ [89,136,139]. Each oxygen ion vacancy leaves behind two electrons as per the following reaction written in the Kröger-Vink notation [89]:

$$O_0 \Leftrightarrow 1/2O_2 + V_0^{\cdot\cdot} + 2e' \qquad \ldots\ldots(2.1)$$

where O_o is the oxygen atom, $V_o^{\cdot\cdot}$ represents oxygen vacancies with two net positive charges and e´ stands for electron with negative charge (´). Electrons released due to oxygen ion vacancy may be captured by Fe^{3+} of $BiFeO_3$ leading to its reduction to Fe^{2+}:

$$Fe^{3+} + 1e' \Leftrightarrow Fe^{2+} \qquad \ldots\ldots\ldots (2.2)$$

The presence of Fe^{2+} and Fe^{3+} ions leads to hopping of electrons as a result of which the conductivity increases. In case of our samples, the resistivity of undoped $BiFeO_3$ at room temperature is $1.6 \times 10^7 \Omega$ cm while it increases by three orders of magnitude to $1.09 \times 10^{10} \Omega$ cm in the Mn-doped $BiFeO_3$ samples. This observation is in agreement with findings of other workers also for Mn-doping level less than 3 atom % [136–142,206–212]. Similarly, we find that the dielectric loss (tanδ) decreases quite significantly from tanδ ~ 0.969 to ~ 0.425 (at 100 kHz) as result of Mn-doping. Higher doping level (> 3 at %) leads to decrease of the resistivity due to change in the valence states from Mn^{3+} to $Mn^{2+}$of Mn ions for charge compensation and also substitution effect which creates oxygen vacancies as confirmed by XPS, leakage current and XES measurements [137,212–214]. Theoretical [215] and experimental (x-ray absorption fine structure (XAFS) spectra [216] Mössbauer and XPS [217] studies revealed that in Mn-doped $BiFeO_3$ sample the oxidation state of Mn ions is always +3. We believe that Mn^{4+} doping in low concentrations plays the role of accepter in $BiFeO_3$ and compensates the electron charge carriers generated by oxygen ion vacancies. This in turn results in redox

reaction involving capture of electron by Mn^{4+} ion reducing it to Mn^{3+}. The instability of Mn^{4+} (MnO_2 decompose to Mn_2O_3 at 923 K Ref [139]) plays a dual role through redox processes to control or reduce the oxygen ion vacancy formation as per the following redox reactions:

1. $Mn^{4+} + 1e' \rightarrow Mn^{3+}$ (capture the electrons released during oxygen ion vacancy formation)

and/ or

2. $Mn^{4+} + Fe^{2+} \rightarrow Fe^{3+} + Mn^{3+}$ (oxidize Fe^{2+} back into Fe^{3+})

Both the reactions can effectively suppress the conversion of Fe^{3+} to Fe^{2+} due to reduced concentration of oxygen ion vacancies and thereby suppress the hopping conductivity. The observed increase in the resistivity and decrease in the tanδ of the doped samples with respect to the undoped samples is therefore seem to be correlated with suppression of oxygen ion vacancy and Fe^{2+} ion concentrations.

We used XPS studies on both the undoped and Mn-doped $BiFeO_3$ samples to determine the Fe^{2+} ion concentrations. As discuss in previous section 2.4.1 that the iodometric titrations give oxygen contents of 2.94 ± 0.02 and 2.98 ± 0.02 for undoped and doped samples, respectively. Evidently, the oxygen ion vacancy concentration is lower in the doped samples. As a result of reduced oxygen ion concentration due to Mn-doping, the redox reaction given by (2) is expected to be suppressed leading to lower Fe^{2+} ion concentration. This was further verified by XPS measurements using Fe 2p core level spectra for both undoped and Mn-doped $BiFeO_3$ samples (see Fig. 2.4(a) and (b)). It is well known that due to spin-orbit coupling, the Fe 2p core level spectra split into two components $2p_{3/2}$ (located at 710.6 eV) and $2p_{1/2}$ (located at 723.5 eV) with a satellite peak located around 719 eV [218–220]. The asymmetry in the peaks towards the lower binding energy in Figs. 2.4(a) and (b) reveals the presence of Fe^{2+} in both the undoped and Mn-doped $BiFeO_3$ samples. In order to quantify the ratio of Fe^{3+}/Fe^{2+}, we have

carefully analyzed the $2p_{3/2}$ peak for both undoped and Mn-doped $BiFeO_3$ samples and the best fits are shown in the insets to Fig. 2.4(a) and (b). The $2p_{3/2}$ peak in the inset consists of two components corresponding to Fe^{2+} (708.5-709.3 eV) and Fe^{3+} (710.6 eV).

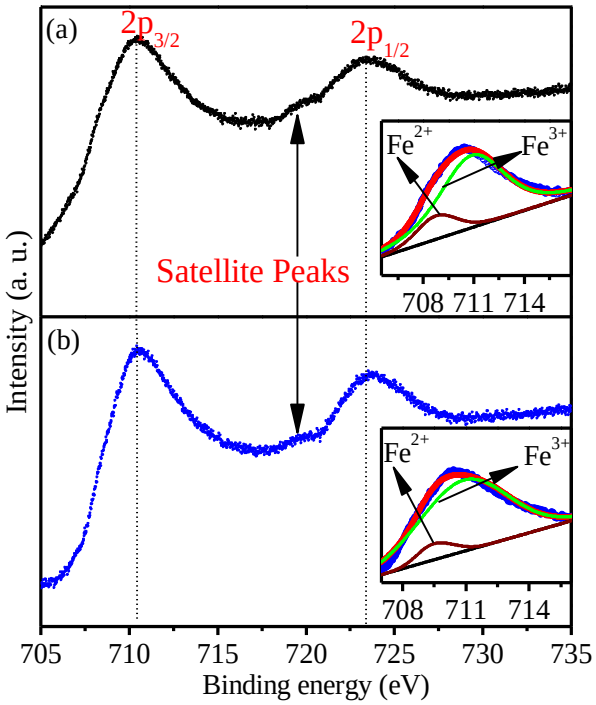

Figure 2.4: XPS Fe 2p core level spectra for **(a)** undoped $BiFeO_3$ **(b)** Mn-doped $BiFeO_3$. Insets to figure 3**(a)** and **(b)** depict the fitted profile of $2p_{3/2}$ peak.

The ratio of Fe^{3+}/ Fe^{2+} for undoped $BiFeO_3$ was found to be 85/15 and for the Mn-doped sample this comes out to be 92/08. The larger concentration of Fe^{2+} ions in undoped $BiFeO_3$ sample is attributed to redox reaction caused by the capture of electron released during oxygen ion vacancy formation as per reaction (1) at high temperatures during sintering. These results along with EDX and iodometric titration analysis give the overall formula as $BiFe^{3+}_{0.88}Fe^{2+}_{0.12}O_{2.94}$ and $BiFe^{3+}_{0.925}Fe^{2+}_{0.06}Mn^{3+}_{0.015}O_{2.98}$, respectively, for the undoped and doped sample assuming that all of Mn has gone into the Fe sites. The ratio of Fe^{3+}/ Fe^{2+} by XPS study show very close proximity with the electronic configuration of our samples as determined by taking charge neutrality and oxygen stoichiometry into the consideration. Thus, our results

clearly reveal a close correlation between Mn-doping and oxygen ion vacancy and Fe^{2+} ion concentrations leading to three order of magnitude increase in the resistivity and significant decrease in tanδ value of the Mn-doped samples with respect to the undoped samples. We now proceed to show the effect of Mn-doping with reduced oxygen ion vacancy and Fe^{2+} concentrations on the low temperature magnetic transitions of $BiFeO_3$.

2.4.4 Effect of Mn doping on the low temperature magnetic phase transitions:

Fig. 2.5 shows the variation of dc magnetization (M (T)) with temperature under ZFC and FC conditions for the undoped and doped samples, respectively, for an applied field of 500 Oe. The ZFC and FC magnetizations bifurcate above 300 K for the undoped samples whereas for the doped samples it begins around 270 K. The bifurcation of the M (T) plots under ZFC and FC conditions increases with decreasing temperature suggesting spin-glass or superparamagnetic behaviour in $BiFeO_3$ at low temperatures as proposed by previous workers also [102,108]. The ZFC and FC magnetization curves of both the samples in the 300 to ~150 K range are consistent with conventional antiferromagnetic (AFM) behaviour in which magnetization is expected to decrease with decreasing temperature below T_N which is close to~650 K for both undoped and doped samples (see Fig. 2.5(b) and (d)). However, both types of samples show an upturn in magnetization below ~150 K. This can happen as a precursor effect to an impending phase transition and accordingly a spin reorientation transition [111,112,116], similar to that in orthoferrites [221,222], with the involvement of electromagnons [111,116], has been proposed [102]. Such a spin reorientation transition has recently been reported in monoclinic compositions of solid solutions of $BiFeO_3$ with $PbTiO_3$ but the transition temperature is well above the room temperature and just below the T_N [223]. In pure $BiFeO_3$, the situation is quite different as spin reorientation has been proposed well below room temperature.

In addition to the transition around 150K due to electromagnon [111,116], the M(T) measurements clearly reveal another anomaly around 260 K in the doped samples (see Fig. 2.5(b)) which is less clear in the undoped samples. A similar anomaly has been

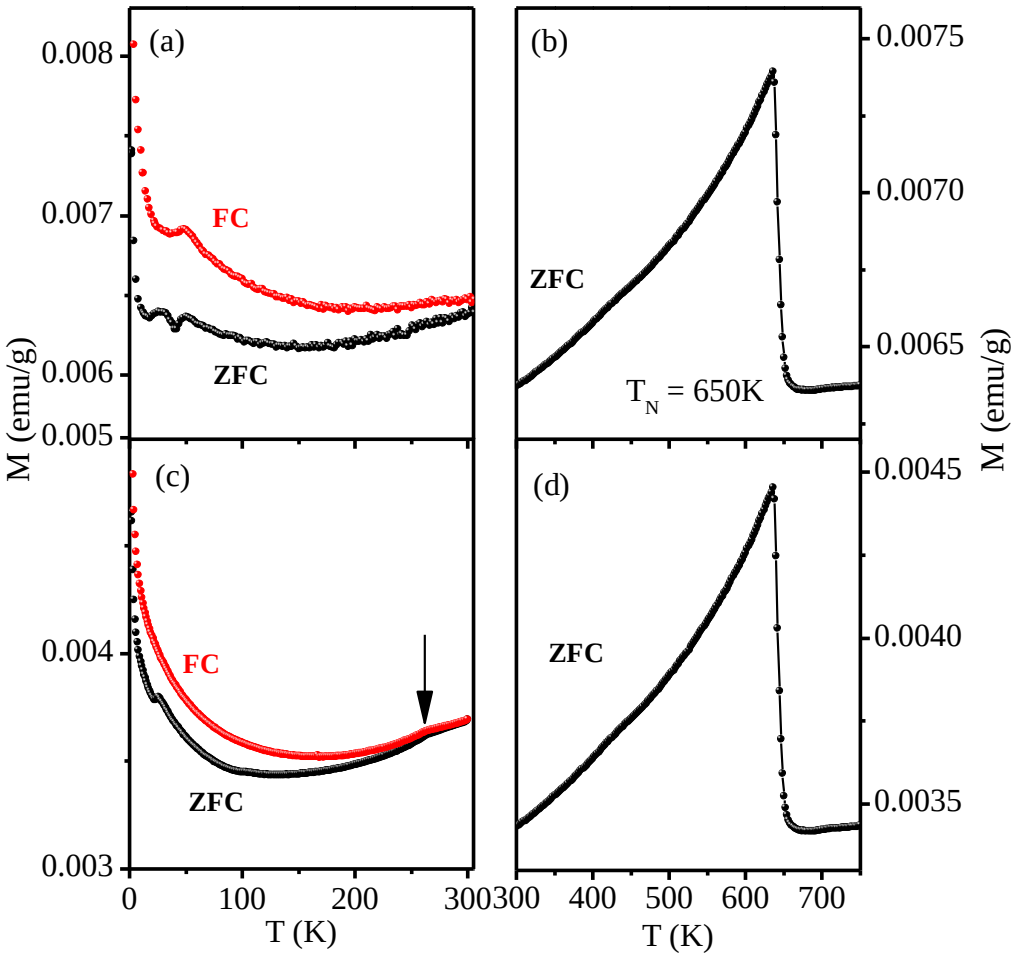

Figure 2.5: Temperature dependence of dc magnetization for **(a-b)** Undoped $BiFeO_3$ and **(c-d)** Mn- doped $BiFeO_3$ at an applied field of 500 Oe in two separate measurements from 2-300K and 300 to 750K range.

reported by Ramachandran et al. [103] also who attributed it to spin-glass transition. We shall discuss the nature of this transition further in the next chapter in more detail. On cooling below 150 K, the ZFC M(T) of undoped samples shows a very prominent peak around 50K but this transition is absent in the doped samples. This transition has been reported by a few workers in the past [87,102] and has been proposed to be due to spin-

glass freezing or superparamagnetic (SPM) blocking since the FC M(T) plot shows clear bifurcation around the peak temperature (~50K) in the ZFC plot of the undoped samples. The peak around 25 K in the ZFC M(T) of both types of sample is not present in the FC M (T) plots of these samples suggests that it could be due to spin glass freezing or superparamagnetic blocking. Below 10 K, both ZFC and FC curves for both types of samples show increase in the magnetization indicating a weak ferromagnetic behaviour of $BiFeO_3$ at such low temperatures, as noted by previous workers also [102,103].

A frequency dependent peak in ac susceptibility (χ' (ω, T)) has been reported around 25K in the literature [102] which has been attributed to spin-glass freezing. Accordingly, we also carried out ac susceptibility measurements χ (ω, T). Fig. 2.6 (a, b) and (c, b) show the real (χ' (ω, T)) and imaginary (χ'' (ω, T)) parts of χ(ω, T) measured

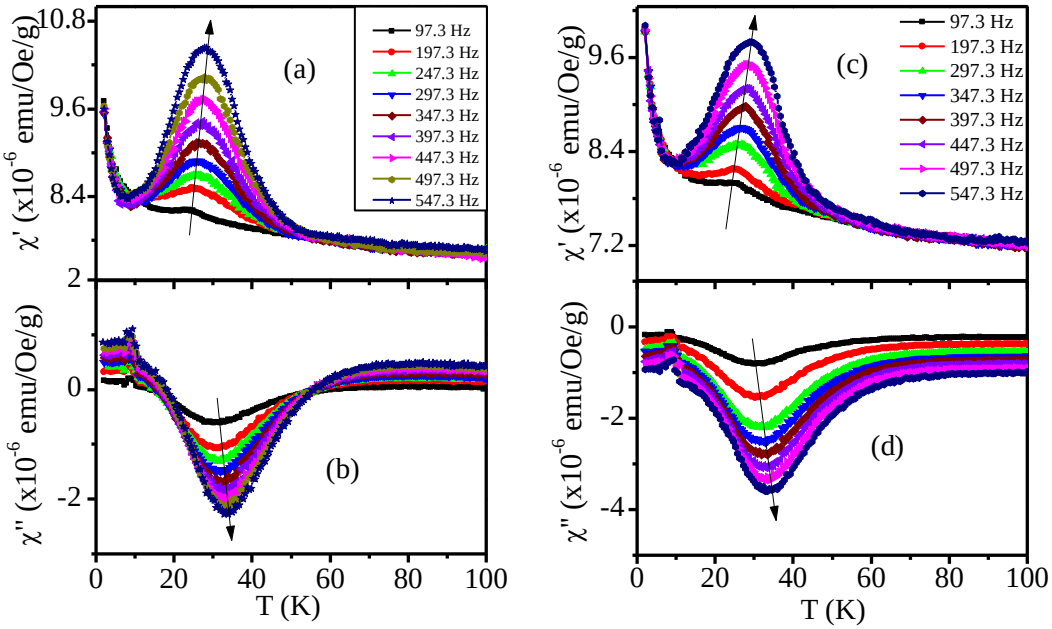

Figure 2.6: Temperature dependence of the real and imaginary parts of the ac susceptibility at various frequencies at an applied ac field of 5 Oe for (**a**, **b**) undoped $BiFeO_3$ and (**c**, **d**) Mn-doped $BiFeO_3$.

with an applied ac drive field of 5 Oe in the frequency range 97.3 Hz to 547.3 Hz for undoped and doped $BiFeO_3$, respectively. It is evident from the figures that the peak temperatures corresponding to the χ' (ω, T) and χ'' (ω, T) shift towards higher temperatures with increasing frequency which can be due to SG freezing or SPM blocking. For SPM blocking, ln τ versus 1/T plot should be linear as per Arrhenius law [224] ($\tau = \tau_0 \, exp\left(\frac{E_a}{k_B T}\right)$ where E_a is activation energy). The spin relaxation time τ can be determined from the measurement frequency (ω =2πf) at the peak temperature (T_f) of χ' (ω, T). The non-linear nature of the plots shown in the insets of Fig. 2.7 (a) and (b) rules out SPM blocking in $BiFeO_3$ at low temperatures. The power law [225] ($\tau = \tau_0 \left(\frac{T_f - T_{SG}}{T_{SG}}\right)^{-z\nu}$ type critical dynamics provides excellent fit for both the undoped and doped samples, as can be seen from Fig. 2.7 (a) and (b), confirming the SG freezing with a T_{SG} ≈ (20±1)K. Our results thus confirm unambiguously that the anomaly observed around T_f ~ 25 K in $BiFeO_3$ is due to SG freezing with a T_{SG} ≈ (20±1)K at which the ergodicity is broken. Our results also show that the earlier report [102] of $T_{SG} > T_f$ in $BiFeO_3$ is not correct and may be an artifact of numerical fit. By definition also, the T_{SG} cannot be higher than $T_f(\omega)$ as it corresponds to the value of $T_f(\omega)$ in the limit of ω tending towards zero at which the slowest spin dynamics diverges. The difference between the M(T) behaviour of the undoped and doped $BiFeO_3$ samples is the absence of the 50K transition and clearer evidence for another transition around 260K in the doped samples. Some weak signatures of a possible transition around 260K has been reported by the previous workers also in undoped samples [103] but it becomes very clear in the doped sample (see Fig.2.5(a) and (c)). The fact that the signatures of these two transitions could be observed unambiguously in M(T) plots of the doped samples highlights the role of Mn-doping and associated decrease in the oxygen ion vacancy and Fe^{2+} ion concentrations in

capturing this transition as discussed in section 2.4.5, both doped and undoped samples exhibit a dielectric step around the 260K with a peak in the loss tangent (tanδ) suggesting

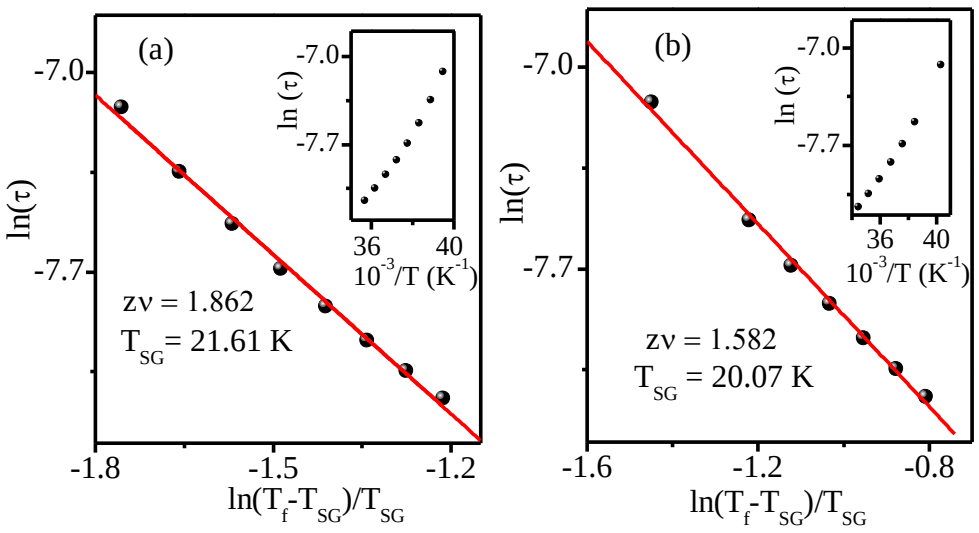

Figure 2.7: ln(τ) vs ln(T_f-T_{SG}/T_{SG}) plot. The solid line is the fit for the power law for **(a)** undoped $BiFeO_3$ **(b)** Mn-doped $BiFeO_3$. Insets depicts ln(τ) vs 1/T plot.

the presence of this transition in both the samples with magnetodielectric couplings. Our magnetization measurements thus suggest that the transition around 25, upturn around 150K and the step around 260 K observed in the ZFC M (T) plot of the doped sample are intrinsic to $BiFeO_3$.

What could be responsible for the 50K transition in the undoped samples and its absence in the doped samples. The iodometric and XPS studies on undoped and doped samples clearly reveal the difference in the defect chemistry of the two samples in terms of decrease in oxygen ion vacancy and Fe^{2+} ion concentrations, respectively, in the doped samples with respect to the undoped samples. The three orders of magnitude increase in the resistivity and decrease in tanδ of the doped sample as compared to that of the undoped samples provides additional credence to the possible role of Mn-doping through reduction in the oxygen ion vacancy and Fe^{2+} ion concentrations. Hence, we believe that

the absence of the 50 K transition in the doped samples of $BiFeO_3$ is most likely due to the neutralization of charged oxygen ion vacancies through Mn-doping.

Defect-induced magnetism is well known phenomenon in solids, in general, and the role of oxygen ion vacancies, in particular, in magnetic as well as non-magnetic materials has been investigated extensively, both experimentally [226–230] and theoretically [231–234]. The oxygen ion vacancies have been reported to influence the magnetic behavior of oxides in several ways. For example, the Fe^{3+} to Fe^{2+} redox reaction has been proposed to create local ferromagnetic clusters via double exchange mechanism that may enhance the magnetization. Using first principle calculations, [232] showed that intrinsic oxygen ion vacancies indeed lead to the formation of Fe^{2+}, as evident from the qualitative differences in the local density of states and promote ferromagnetism. The fact that the magnetization of the undoped samples shown in Fig. 2.5(a) is higher than that of the doped sample (see Fig. 2.5(c)) agrees well with this picture.

2.4.5 Evidence for change in dielectric constant around the magnetic transitions:

The appearance of an anomaly in the dielectric constant and/or loss tangent around a magnetic transition is a signature of magnetoelectric coupling [68,89], in the absence of space charge contribution coming of Fe^{2+}/Fe^{3+} redox reaction [117]. The space charge effect is minimized at higher frequencies [89] in $BiFeO_3$ based samples. The variation of the real part of the dielectric constant (ε') and loss tangent ($\tan\delta$) for undoped and Mn-doped $BiFeO_3$ as a function of temperature is shown in Figs. 2.8 (a, b) and 2.9 (a, b) at 20 kHz. The real part of ε' shows a change of slope around 25 K for both undoped and Mn-doped $BiFeO_3$ samples as shown in the inset of Figs. 2.8 (a) and 2.9(a) for the undoped and Mn-doped $BiFeO_3$ samples at 20 kHz. This suggests that the transition around 25 K, observed by M(T) measurement may involve magnetoelectric coupling also. Also, since the Mn-doping reduces oxygen ion vacancies, it would lead to suppression of

space charge dipole. This indeed is reflected in the lower values of ε′ and tanδ of the doped sample shown in Fig. 2.9. One also observes a prominent dielectric step around 260K transition [117] with a peak in the tanδ plot in both the doped and undoped samples. This not only suggests the presence of magneto-dielectric coupling for 260K transition

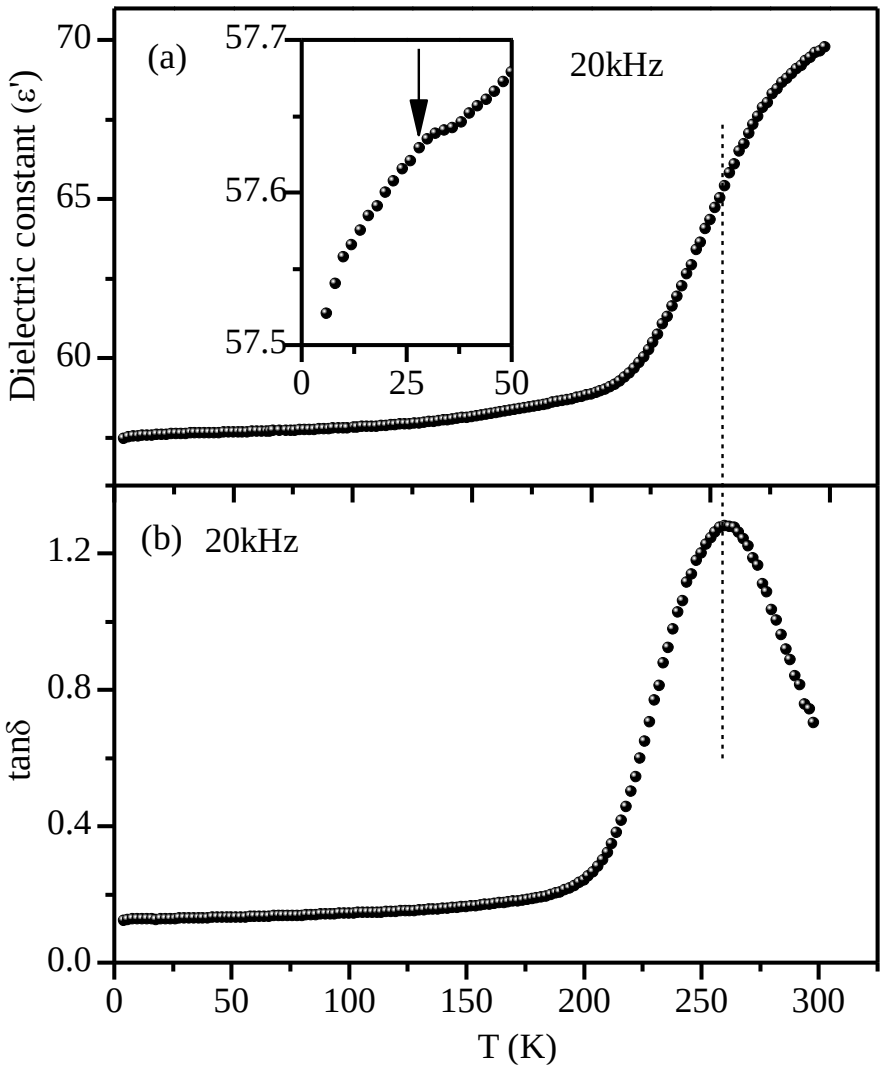

Figure 2.8: Dielectric constant and dielectric loss as a function of temperature for undoped $BiFeO_3$ at 20 kHz frequency. Inset to figure show the anomaly around 25K.

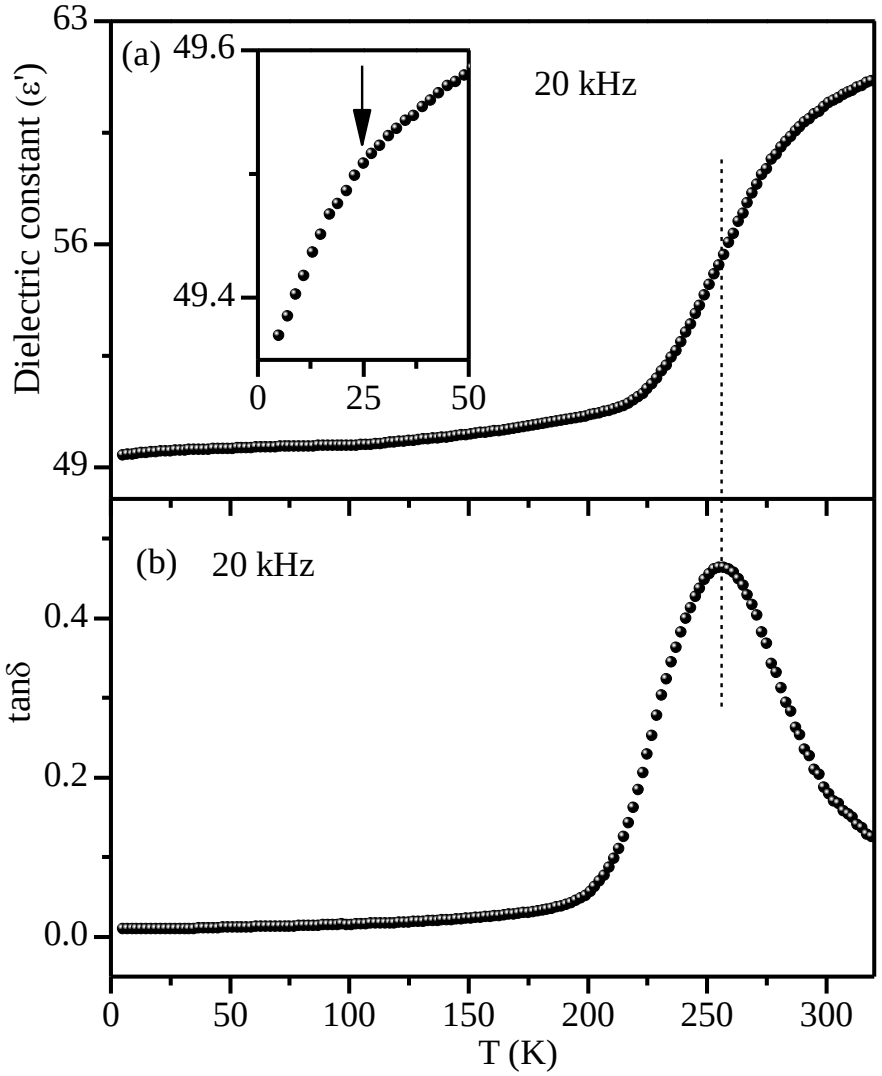

Figure 2.9: Dielectric constant and dielectric loss as a function of temperature for Mn-doped $BiFeO_3$ at 20 kHz frequency. Inset to figure show the anomaly around 25K.

but also provides indirect support to the presence of this transition in undoped sample, not clearly revealed in the M (T) plot (see Fig. 2.5(a)). The observation of a relaxation step and a change of slope 260K and 25 K, transitions in both types of samples suggests magneto-dielectric coupling.

2.4.6 Evidence for change in unit cell parameters around the magnetic transitions:

In order to verify if any one of the low temperature magnetic transitions involves a structural change, we carried out XRD studies in the 300 to 13 K temperature range. Fig.

2.10 and 2.11 shows the temperature dependent evolution of XRD profiles of a few selected peaks (222_{pc}, 400_{pc} and 440_{pc} reflections) after stripping off the $K_{\alpha 2}$ contribution

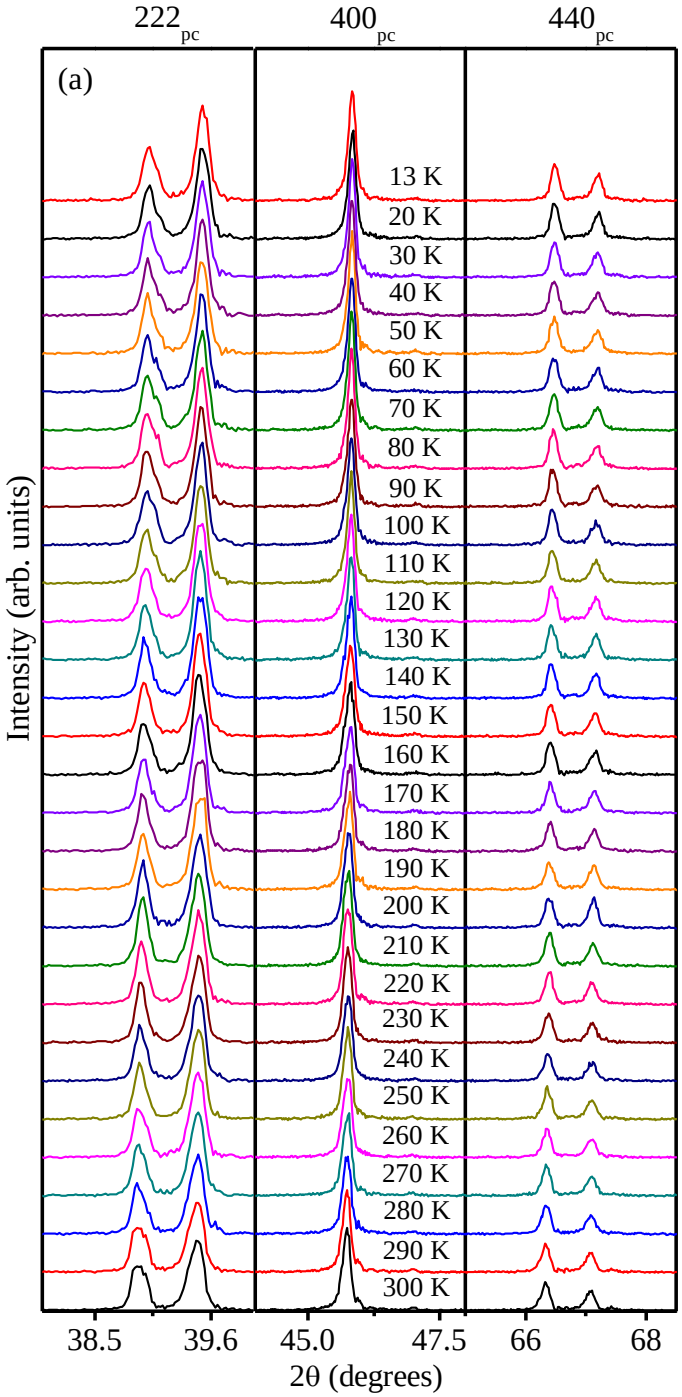

Figure 2.10: The evolution of x-ray powder diffraction profiles of the $(222)_{pc}$, $(400)_{pc}$ and $(440)_{pc}$ reflections of pure $BiFeO_3$ sample with temperature showing the absence of any structural phase transition. The Miller indices are written with respect to a doubled pseudocubic cell.

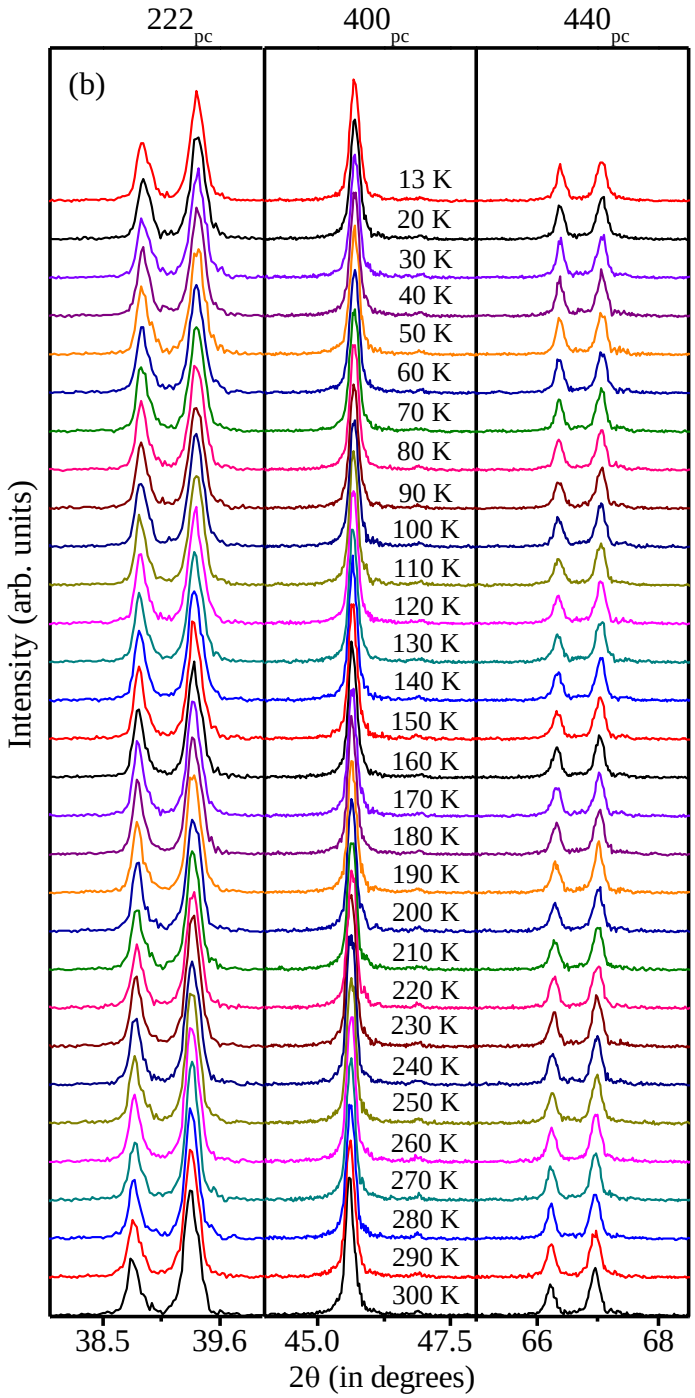

Figure 2.11: The evolution of x-ray powder diffraction profiles of the $(222)_{pc}$, $(400)_{pc}$ and $(440)_{pc}$ reflections of Mn-doped $BiFeO_3$ sample with temperature showing the absence of any structural phase transition. The Miller indices are written with respect to a doubled pseudocubic cell.

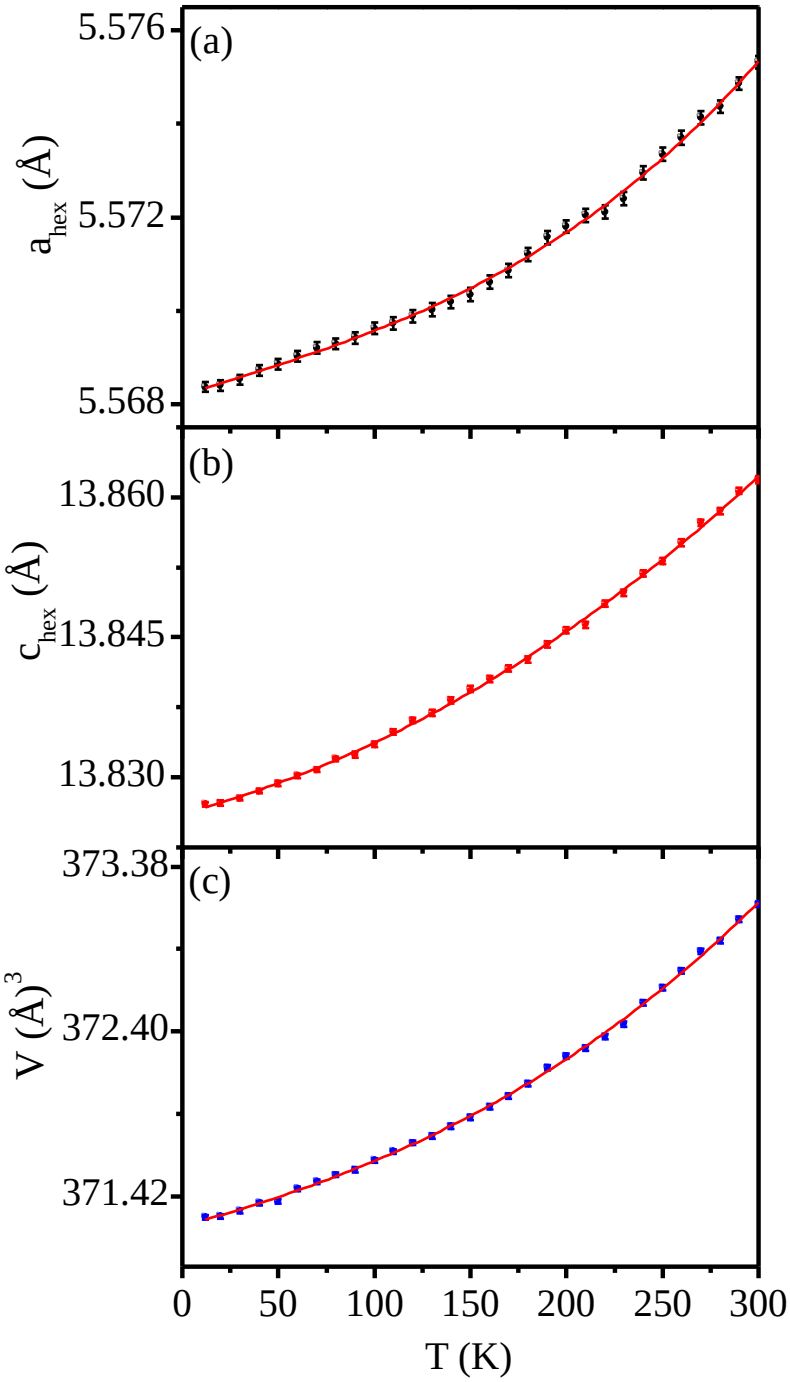

Figure 2.12: Variation of unit cell parameters (a_{hex}, c_{hex} and V_{hex}) with temperature obtained from the LeBail refinement of the x-ray powder diffraction data for pure $BiFeO_3$ sample.

for both the undoped and Mn-doped $BiFeO_3$. It is evident from the figures that no new peaks appear or disappear in the investigated temperature range 13 K-300 K. This implies that the crystal structure remains rhombohedral in the R3c space group and that there is no structural phase transition in the temperature range from 13 K to 300 K. The variation

of lattice parameters (a_{hex} and c_{hex}) and unit cell volume (V_{hex}) of the hexagonal unit cell, as obtained from the LeBail analysis of XRD data, with temperature is shown in Figs. 2.12 (a-c) and 2.13(a-c) for undoped and Mn-doped samples, respectively.

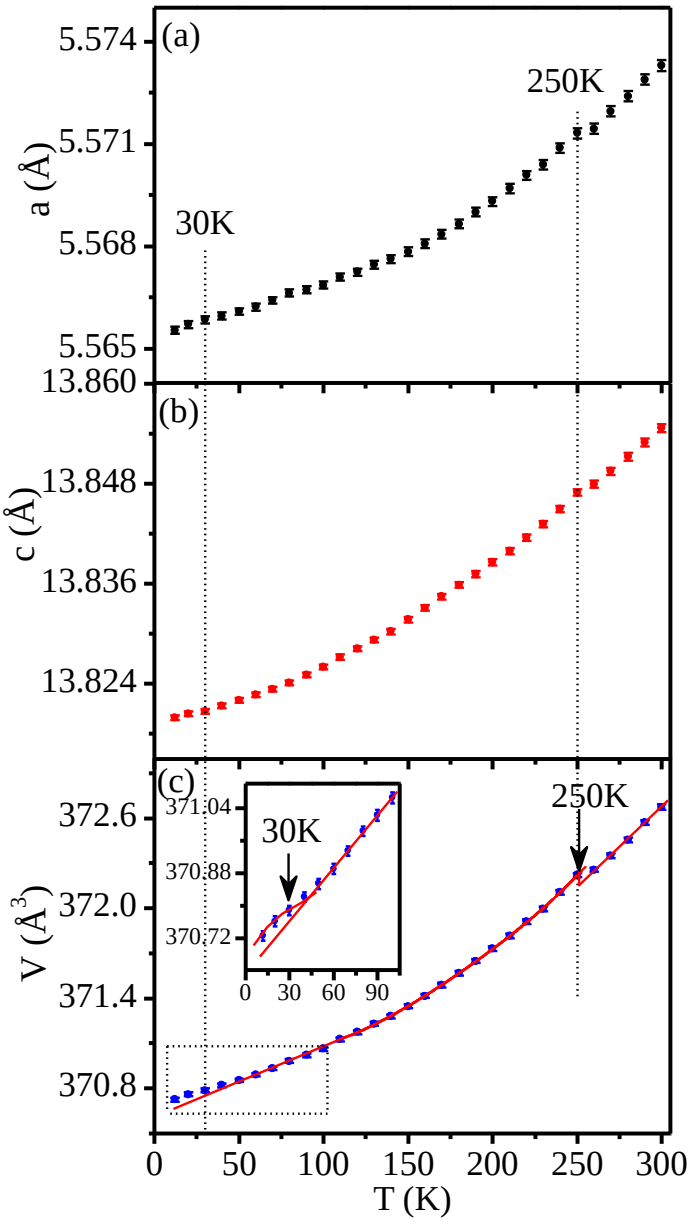

Figure 2.13: Variation of unit cell parameters (a_{hex}, c_{hex} and V_{hex}) with temperature obtained from the LeBail refinement of the x-ray powder diffraction data for Mn doped $BiFeO_3$ sample.

The unit cell parameters gradually decrease with decreasing temperature for both types of samples. However, the temperature variation of cell parameters and unit cell volume of Mn-doped $BiFeO_3$ sample shows a clear change of slope around 30 K and

250K. In case of undoped sample, this change of slope is not clear. Thus Mn-doping helps in revealing these weak anomalies in the unit cell parameters while in the undoped samples these transitions are masked due to higher oxygen in vacancies. The observation of anomaly in the unit cell parameters around the two magnetic transitions suggests magneto-elastic coupling [189,235,236].

2.4.7 Anomalous ac susceptibility response of $BiFeO_3$:

Having established the existence of a spin glass freezing around 25K in both types of samples of $BiFeO_3$, we now turn to some intriguing aspects of ac susceptibility $\chi(\omega, T)$ around this transition. Firstly, the peak height of $\chi'(\omega, T)$ increases with increasing frequencies which is unusual as the susceptibility always decreases with increasing frequency except near frequencies corresponding to a resonant absorption that may be linked with the resistance, capacitance and inductance of the entire circuit rather than just the sample. In principle, it is possible to push the resonance frequencies to higher side by reducing the capacitance and inductance of the circuit by reducing the sample quantity. However, this was not possible in $BiFeO_3$ due to very weak signal for the $\chi'(\omega, T)$. A similar anomalous ac magnetic susceptibility data has been reported even in single crystal samples of $BiFeO_3$ [102]. It is also important to note that the imaginary part $\chi''(\omega, T)$ shows negative cusps at T_f with a peak temperature above the corresponding peak temperature for the real part $\chi'(\omega, T)$. The negative value clearly suggests that the circuit is no longer purely inductive except at very low temperatures (< ~10K). The third intriguing aspect of the $\chi''(\omega, T)$ is the presence of a tiny peak around 10K below which the imaginary part shows positive value. All these features require further study, as some of these anomalous features have also been tentatively attributed to the coexisting modulated magnetic structure of $BiFeO_3$ [102], not observed in the conventional spin glass systems. We shall return to the possible role of spin cycloid in causing this

anomalous frequency dependence of $\chi(\omega, T)$ in the next chapter. What is even more intriguing is the occurrence of a spin-glass phase in a homogeneously ordered system like $BiFeO_3$ without any quenched impurity and randomness as the existing models of spin-glass transitions are based on the concept of disorder, randomness and frustration [24,41–45]. In recent years, several compounds with geometrical frustration have been reported to exhibit spin glass transition in the absence of any apparent disorder [118–124]. But source of frustration in $BiFeO_3$ is not obvious. We believe that the spin glass transition may be caused by competing nearest and next-nearest neighbour interactions. But the existing density functional theory (DFT) give very small value J_2 (0.29 meV) as compared to J_1 (6.48 meV) [237]. The calculations need to be revisited in future.

2.4.8 Ground state of $BiFeO_3$:

$BiFeO_3$ shows non-collinear AFM ordering with Heisenberg spins with an incommensurately modulated cycloidal spin structure superimposed on it. Recent neutron scattering [73–75,100,101] and NMR studies [96–99] suggest that this spin cycloid is stable down to the lowest temperature (~5K). Considering these observations in conjunction with the present results, the most likely scenario for the ground state of $BiFeO_3$ is the coexistence of the spin glass phase and the long range ordered spin cycloid. The coexistence of LRO AFM and spin glass state has been a subject of extensive theoretical and experimental investigations for both Ising and Heisenberg systems [49–53]. In some of the Heisenberg systems, it has been predicted theoretically [51–53] and verified experimentally [172,238–243] that the coexistence is due to the freezing of the transverse component of the spins. An alternative proposal in disordered systems like $PbFe_{0.5}Nb_{0.5}O_3$ (PFN) whereby the two phases result from two different magnetic sublattices, one (LRO) with percolative path ways and the other due to isolated Fe-O-Fe clusters, has also been proposed [171]. In $BiFeO_3$ has no quenched disorder per say,

except for the possibility of Fe^{2+} ions in the magnetic sublattice replacing some of the Fe^{3+} sites due to redox reaction caused by oxygen vacancies and raising the possibility of local ferromagnetic interactions via double exchange. In the absence of disorder in the magnetic sublattice or any frustrated interaction between the spins, the most likely possibility for the emergence of the spin glass phase is due to the freezing of the transverse component of the spins. Local magnetic probe like NMR [96–99] and the global probes like neutron scattering [73–75,100,101] have revealed the possibility of distortions in the long range ordered magnetic modulated structure even though the extent of distortion from harmonic modulation is much less for the average structure, probed by the bulk techniques like neutron scattering, than that reported by local probe like NMR. Whether this anhormonicity is linked with the gradual transverse freezing of the spins or not needs further investigation using neutron scattering studies on single crystals. We shall return to transverse freezing aspect in the next chapter at greater length.

2.5. Conclusions:

$BiFeO_3$ samples were synthesized by conventional solid-state route with and without 0.3wt% MnO_2 doping and characterized for their phase purity and crystal structure, microstructure and composition using synchrotron x-ray diffraction, SEM and EDX techniques. A comparative iodometric titration and XPS study of undoped and Mn-doped $BiFeO_3$ reveals that the oxygen ion vacancy and Fe^{2+} ion concentrations decrease significantly as a result of Mn doping. Based on the results of dc magnetization M(T), AC susceptibility χ (ω, T), dielectric constant ε' (ω, T) and XRD studies in conjunction with iodometric titration and XPS studies on the undoped and doped samples, we conclude that the low temperature transitions of $BiFeO_3$ occurring around 25 K, 150 K and 260 K are intrinsic to $BiFeO_3$ as they are present in both the samples. Our results show that the

magnetic transition around 50 K reported by earlier workers, is absent in Mn-doped $BiFeO_3$ and results in the undoped sample due to oxygen vacancies.